

Low-temperature pulverization-specific *Sargassum horneri* extract accelerates wound healing and attenuates inflammation in a mouse burn model

Eunguk Shin^{a*}, Hee-Tae Kim^{b*}, Haksoo Lee^c, Byeongsoo Kim^c, Junhyeong Park^c, Sujin Park^c, Soomin Yum^c, Seoul-Ke Kim^d, Jae-Myung Lee^{b,d} and BuHyun Youn^{a,c,e}

^aNuclear Science Research Institute, Pusan National University, Busan, Korea; ^bDepartment of Naval Architecture and Ocean Engineering, Pusan National University, Busan, Korea; ^cDepartment of Integrated Biological Science, Pusan National University, Busan, Korea; ^dHydrogen Ship Technology Center, Pusan National University, Busan, Korea; ^eDepartment of Biological Sciences, Pusan National University, Busan, Korea

ABSTRACT

Burn injuries, affecting local skin disruption as well as inducing systemic inflammatory responses, are presented as a global public health problem. To enhance the effects of burn wound healing, treatment must simultaneously regulate both re-epithelialization and hyperinflammation. Extracts of *Sargassum horneri* (*S. horneri*) have shown a potential to enhance skin wound healing through antioxidative properties, immune enhancement, and modulation of inflammatory responses. However, despite its promising application for burn wound healing, specific investigation into *S. horneri*-derived compounds for enhancing wound healing has not yet been conducted. In this research, we investigated the burn wound-healing effect of the low-temperature pulverization-specific *S. horneri* extract (LPSHE), which could not be detected using the room-temperature grinding method. In a mouse burn model with third-degree burn injuries, LPSHE accelerated re-epithelialization by promoting the increase in F-actin formation and reduced burn-induced ROS levels. Additionally, LPSHE significantly regulated hyperinflammation by reducing pro-inflammatory cytokines. Further investigation into molecular mechanisms using HaCaT keratinocytes also demonstrated beneficial effects on burn wound healing. Taken together, our findings suggested that LPSHE is a promising therapeutic candidate for enhancing burn wound healing. Furthermore, this research underscored the importance of low-temperature pulverization in discovering novel natural compounds from marine organisms.

ARTICLE HISTORY

Received 10 May 2024
Revised 25 July 2024
Accepted 20 August 2024

KEYWORDS

Sargassum horneri; low-temperature pulverization; burn wound healing; antioxidant activity; inflammatory regulation

Introduction

Burn injuries are considered a significant global public health challenge and contribute to an estimated 180,000 deaths annually (Evers et al. 2010; James et al. 2020; Jeschke et al. 2020). The pathophysiology of burns involves the destruction of skin tissues, leading to the generation of oxidative stresses and the release of pro-inflammatory cytokines at the injury site (Parihar et al. 2008; Burgess et al. 2022). To address this multifaceted challenge and enhance burn wound healing, interventions must target re-epithelialization, antioxidation, and systemic inflammation simultaneously.


Marine organisms harbor a wealth of bioactive molecules with potential health benefits, ranging from anti-inflammatory properties to antioxidative and skin-

care effects (Cragg 1998; Matulja et al. 2020; Peñalver et al. 2020; Lomartire and Gonçalves 2023). *Sargassum horneri* (*S. horneri*), a brown seaweed indigenous to East Asia, is known to contain diverse beneficial natural compounds. While various extracts from *S. horneri* have demonstrated promising biological functions such as antioxidation, immune enhancement, and modulation of inflammatory responses, their potential in wound healing, particularly in the context of burn injuries, remains underexplored (Lee et al. 2020; Sanjeewa et al. 2020; Han et al. 2021; Herath et al. 2021; Jung et al. 2022; Kim et al. 2024).

Efficient extraction of natural compounds requires an optimal particle size, achieved through drying at high temperatures and subsequent pulverization

CONTACT Jae-Myung Lee  jaemlee@pusan.ac.kr  Department of Naval Architecture and Ocean Engineering, Pusan National University, Busandaehak-ro 63beon-gil 2, Geumjeong-gu, Busan, 46241, Korea Hydrogen Ship Technology Center, Pusan National University, Busandaehak-ro 63beon-gil 2, Geumjeong-gu, Busan, 46241, Korea; BuHyun Youn  bhyoun72@pusan.ac.kr  Department of Integrated Biological Science, Pusan National University, Busan, 46241, Korea Nuclear Science Research Institute, Pusan National University, Busan, 46241, Korea Department of Biological Sciences, Pusan National University, Busan, 46241, Korea

*These authors contributed equally.

 Supplemental data for this article can be accessed online at <https://doi.org/10.1080/19768354.2024.2396903>.

© 2024 The Author(s). Published by Informa UK Limited, trading as Taylor & Francis Group
This is an Open Access article distributed under the terms of the Creative Commons Attribution-NonCommercial License (<http://creativecommons.org/licenses/by-nc/4.0/>), which permits unrestricted non-commercial use, distribution, and reproduction in any medium, provided the original work is properly cited. The terms on which this article has been published allow the posting of the Accepted Manuscript in a repository by the author(s) or with their consent.

(Nandasiri et al. 2019; Prasedya et al. 2021; Yuan et al. 2023). However, conventional grinding methods may result in the loss of significant fractions of natural components (Balasubramanian et al. 2016; Sharma et al. 2016; Liu et al. 2018). Previous studies employing cryogrinding techniques have shown a substantial improvement in extraction efficacy compared to conventional methods (Sharma et al. 2016; Liu et al. 2018; Jung and Rhee 2020). Nonetheless, cryogrinding poses challenges for industrial-scale applications, necessitating the development of alternative strategies for identifying bioactive compounds from seaweeds (Freitas et al. 2022).

In this study, we aim to identify the novel compounds in *S. horneri* responsible for its potential in burn wound healing. Utilizing the superior extraction efficacy of low-temperature pulverization, we have discovered a novel compound, low-temperature pulverization-specific *S. horneri* extract (LPSHE). We also evaluated the re-epithelialization and attenuating hyperinflammation properties of LPSHE in both mouse models and HaCaT cells. By elucidating the therapeutic properties of LPSHE, we aimed to contribute to the development of novel strategies for burn wound management and underscored the importance of exploring natural resources, such as *S. horneri*, in addressing global health challenges.

Results

Low-temperature pulverization system extracts the novel *S. horneri* compound

To extract novel natural compound from *S. horneri*, we utilized LNG-powered low-temperature pulverization system. This system was previously proposed to perform marine debris recycling with a liquefied natural gas (LNG)-fueled propulsion system (Lee et al. 2021). Using our LNG-pulverizing system, *S. horneri* was pulverized at 24,000 rpm in the chamber that was set to -60°C . Crushed *S. horneri* particles were extracted and concentrated in 50% MeOH, at 60°C (Figure 1(A)). As a result of cryogenic grinding, the size of the crushed particles (approximately 1 mm) was smaller than normal-temperature grinding (approximately 30 mm) (Figure 1(B)). HPLC-UV Chromatogram analysis revealed that the cryogenic grinding-derived *S. horneri* extract contained specific compounds that were not present in the normal-temperature grinding extract (Figure 1(C)). Therefore, we purified the low-temperature pulverization-specific *S. horneri* extract (LPSHE). LPSHE is >95% pure by HPLC analysis.

To characterize structural and molecular information, we analyzed the LPSHE molecular weight, formula, and

structure using Q-TOF LC/MS and proton nuclear magnetic resonance spectroscopy (NMR). From the TOF-MS analysis, we predicted that the calculated molecular weight of the LPSHE was 414.5, and the formula was $\text{C}_{24}\text{H}_{30}\text{O}_6$ (Figure S1A). In the aromatic region (7–9 ppm) from full spectrum of proton NMR data, we characterized that 7 aromatic protons existed, with proton coupling between 8.15 and 7.36 ppm, and between 7.55 and 7.44 ppm (Figure S1B). From these results, we determined that the backbone structure of the LPSHE had two aromatic rings and three side chains (Figure 1(D)).

LPSHE accelerates re-epithelialization on burn-wounded skin

Skin wound healing is classically divided into three phases: inflammation, proliferation, and remodeling (Tiwari 2012; Burgess et al. 2022). In the second and third phases of wound healing, wounded skin undergoes re-epithelialization (Haase et al. 2003; Gurtner et al. 2008; Lim et al. 2023). To determine the re-epithelialization effect of the LPSHE, we established a burn mouse model and measured the burn wound area closure rates (Figure 2(A)). After 14 days, we observed that wounds treated with the LPSHE or Commercial ointment had significantly recovered in the wounded site compared with the non-treated group (Burn vs Burn + Commercial ointment: $p < 0.001$, Burn vs Burn + LPSHE: $p < 0.001$, Burn + LPSHE vs Burn + Commercial ointment: $p = 0.0150$) (Figure 2(B)). To promote the re-epithelialization, a collagen layer must form and recover the skin wound site (Werner et al. 2007; Gurtner et al. 2008). The Commercial ointment or LPSHE had no effect on wound healing in burn-induced skin destruction until 3 days. However, after 14 days, we observed that the collagen formation in the dermis was further increased by treatment with the LPSHE or Commercial ointment (Figure 2(C)). To promote the wound re-epithelialization from the surrounding wound margins toward the center, keratinocytes increase the F-actin formation and increase keratinocyte migration (Krishnaswamy and Korrapati 2014; Rodrigues et al. 2019; Peña and Martin 2024). Phalloidin staining showed that the LPSHE or Commercial ointment treatment significantly enhanced F-actin distribution in the injured skin tissue after 3 days (Figure 2(D)). We further determined the expression of heme oxygenase 1 (HMOX1) and fatty acid-binding protein 4 (FABP4) in the wounded skin. HMOX1 has antioxidant and tissue-protective actions. FABP4 helps skin regeneration through fibroblast migration and extracellular matrix production (Lima

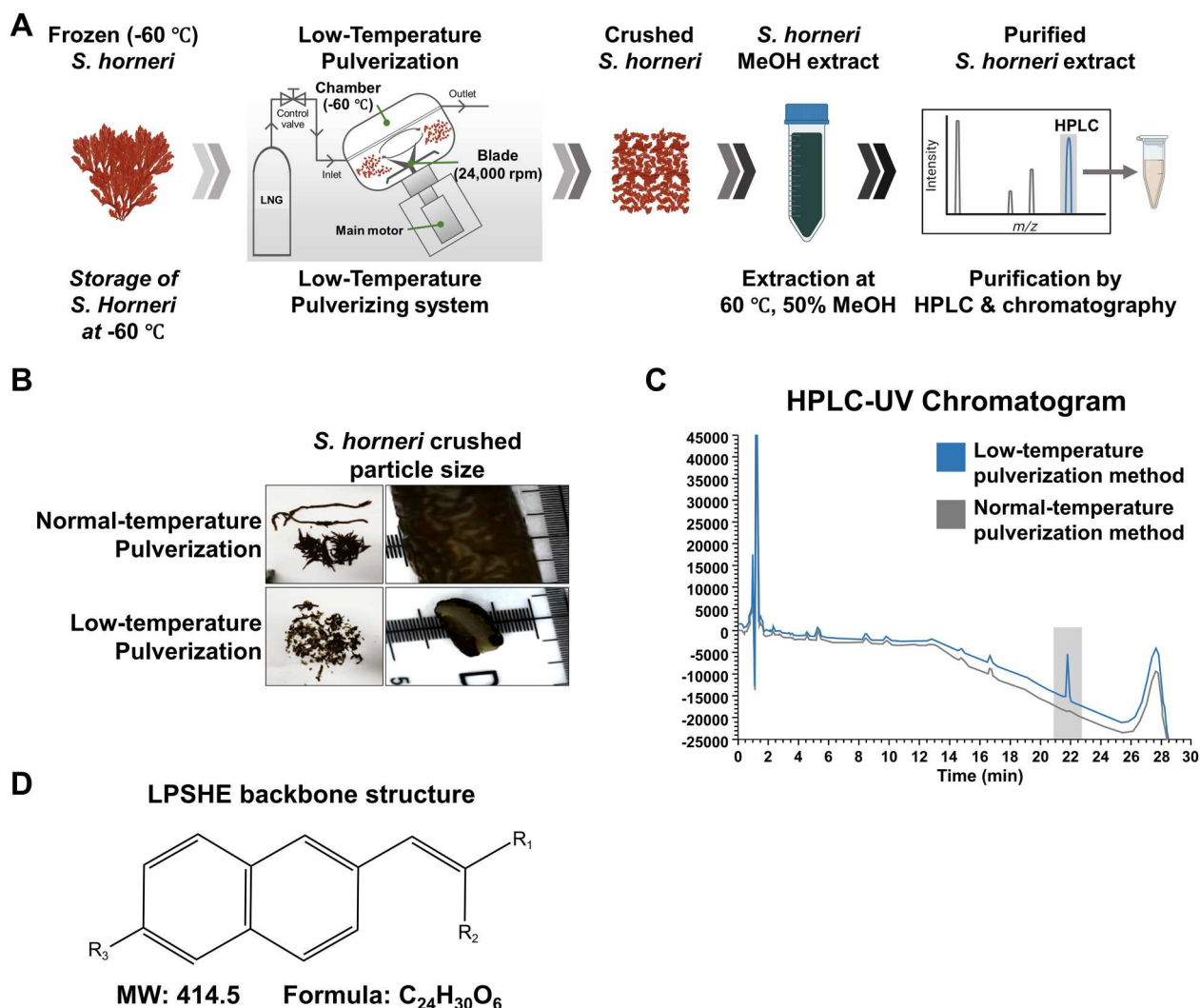


Figure 1. Investigation of low-temperature pulverization-specific component extracted from *S. horneri*: (A) Scheme of upcycling *S. horneri* with low-temperature pulverization. (B) Comparison of crushed particle size of *S. horneri* utilized with normal-temperature pulverization method and low-temperature pulverization method. (C) Comparison of HPLC analysis with normal-temperature pulverization method-derived extract and low-temperature pulverization method-derived extract. Low-temperature pulverization-specific *S. horneri* extract (LPSHE) was marked. (D) Backbone structure of the LPSHE examined with their molecular formula and exact masses.

et al. 2011; Furuhashi et al. 2014; Rivera-Gonzalez et al. 2014; Song et al. 2017). HMOX1 and FABP4 expression levels were increased by burn injury, and the LPSHE or Commercial ointment treatment further increased the FABP4 and HMOX1 levels (Figure 2(E)). Previous studies demonstrated that reducing ROS could be an attractive strategy for enhancing the wound-healing capacity (Parihar et al. 2008; Mittal et al. 2014). We confirmed that the increased ROS levels (nitrotyrosine and 4-hydroxynoneal expression) after burn injury were reduced by LPSHE or Commercial ointment treatment (Figure 2(F)). In addition, blood ROS levels also reduced by LPSHE or Commercial ointment treated groups (Figure 2(G)). Taken together, these burn wound-healing phenotypes demonstrated that LPSHE

has burn wound-healing efficacy similar to Commercial ointment.

LPSHE attenuates hyperinflammation after burn injury

In the first phase of wound healing, acute and local immune responses activate the innate immune response (Engelhardt et al. 1998). However, hyperinflammation of multiple organs causes detrimental effects, disrupting the immune equilibrium and disturbing re-epithelialization (Evers et al. 2010; Burgess et al. 2022; Źwieręto et al. 2023). Therefore, hyperinflammation must be regulated to improve burn wound healing. The burn mouse model was treated with the LPSHE or Commercial

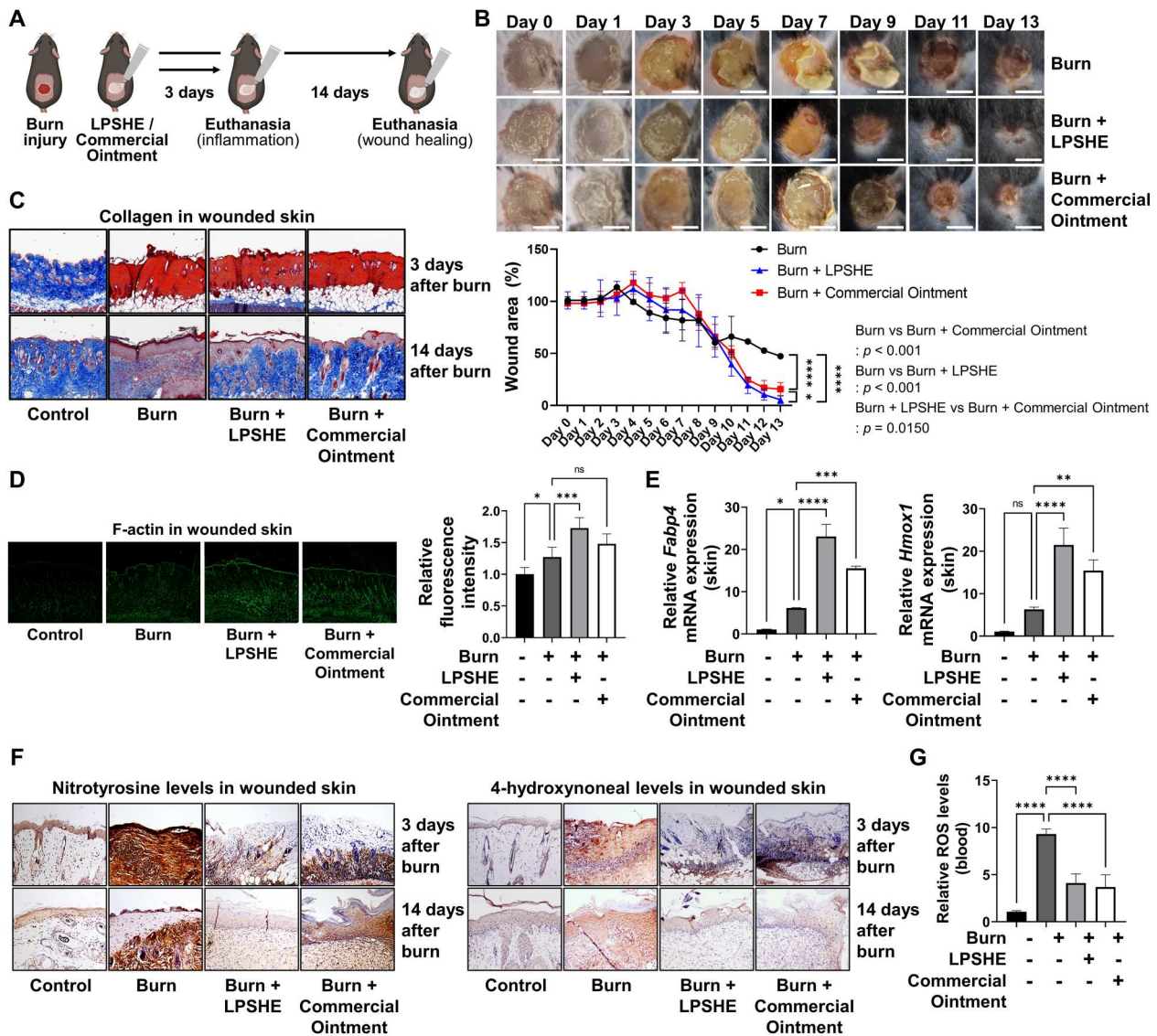


Figure 2. LPSHE accelerates skin wound healing after burn injury: (A) Experimental schedule for burn, LPSHE, and Commercial ointment treatment to burn mouse model. (B) Illustration of wound appearances after 0–13 days after burn injury with LPSHE or Commercial ointment treatment. The curves represent the wound area of each group (Burn vs Burn + Commercial ointment: $p < 0.001$, Burn vs Burn + LPSHE: $p < 0.001$, Burn + LPSHE vs Burn + Commercial ointment: $p = 0.0150$). (C) Wound-healing capacity of LPSHE was confirmed via Masson's trichrome staining (blue: collagen, red: cytoplasm, brown to black: cell nuclei). (D) Effect of LPSHE treatment on the alteration of actin distribution was measured by phalloidin staining. (E) HMOX1 (antioxidant protein) and FABP4 (an adipogenesis marker) expressions in the skin of burn-treated mice were verified by real-time qRT-PCR. (F) IHC results of the two ROS markers, nitrotyrosine and 4-hydroxynoneal, showed decreased ROS levels by LPSHE in the skin of burn mouse model. (G) Relative ROS levels determined by DCF2DA intensity in mice blood samples. Statistical analysis was performed with one-way ANOVA plus a Dunnett's multiple comparisons test for (D), (E), and Student's t -test for (B). ns; non-significant, $*p < 0.05$, $**p < 0.01$, $***p < 0.0005$, $****p < 0.0001$.

ointment for three days after the burn injury (Figure 3(A)). To assess inflammatory responses, we examined the expression level of pro-inflammatory cytokines (IL-1 β , IL-6, and TNF- α) in the liver, lungs, spleen, kidneys, and skin. Increasing pro-inflammatory cytokines after burn injury was alleviated by LPSHE or Commercial ointment treatment (Figure 3(B–D)). The hematoxylin and eosin (H&E) staining results showed that inflammatory infiltrates in the multi-organs were reduced by the

LPSHE or Commercial ointment treatment (Figure 3(E) and Figure S3A). In addition, IHC analysis demonstrated a reduction in CD3⁺ T cell infiltration following the LPSHE or Commercial ointment treatment (Figure 3(F) and Figure S4A). The inflammation score, which was assessed from 0 to 5 by analyzing the degree of infiltration in the H&E staining and IHC results, confirmed that the LPSHE or Commercial ointment regulated hyperinflammation (Figure 3(G) and Figure S4B). These

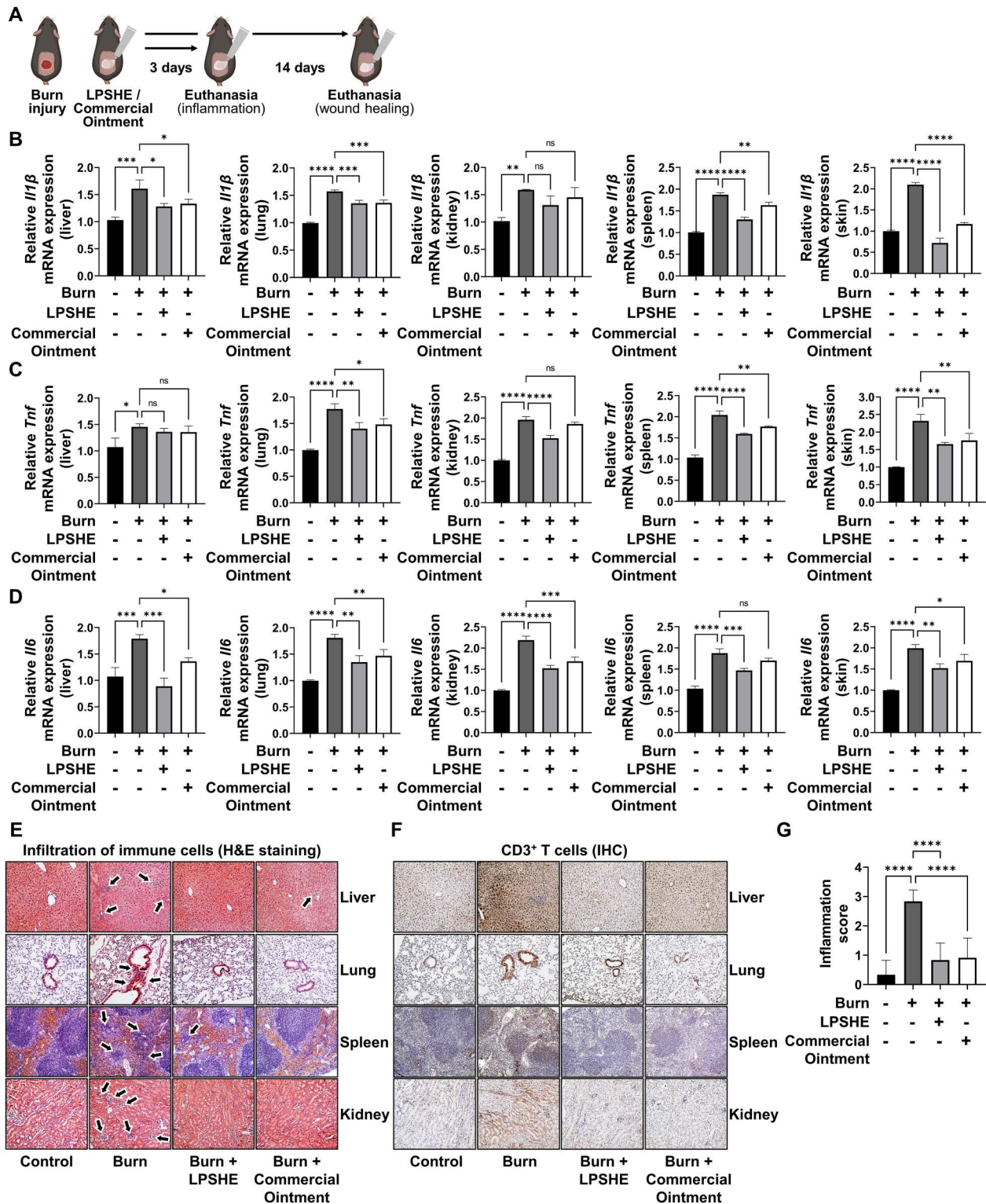


Figure 3. LPSHE alleviates hyperinflammation after burn injury: (A) Experimental schedule for burn, LPSHE, and Commercial ointment treatment to burn mouse model. (B–D) Expression of pro-inflammatory cytokines (IL-1 β , IL-6, and TNF- α) in the liver, lung, spleen, kidney, and skin of burn mouse model was assessed by real-time qRT-PCR. (E) H&E staining results showed that LPSHE or Commercial ointment treatment alleviated burn-induced inflammation. Arrows indicate inflammatory infiltrates (magnification: X200). (F) IHC analysis showed infiltration of CD3⁺ T cell in the organs (magnification: X200). (G) Inflammation scores were evaluated based on the inflammatory infiltration observed in histological analysis of Figure 3(E and F) (from 0 score to 5 score). Statistical analysis was performed with one-way ANOVA plus a Dunnett's multiple comparisons test. ns; non-significant, * $p < 0.05$, ** $p < 0.01$, *** $p < 0.0005$, **** $p < 0.0001$.

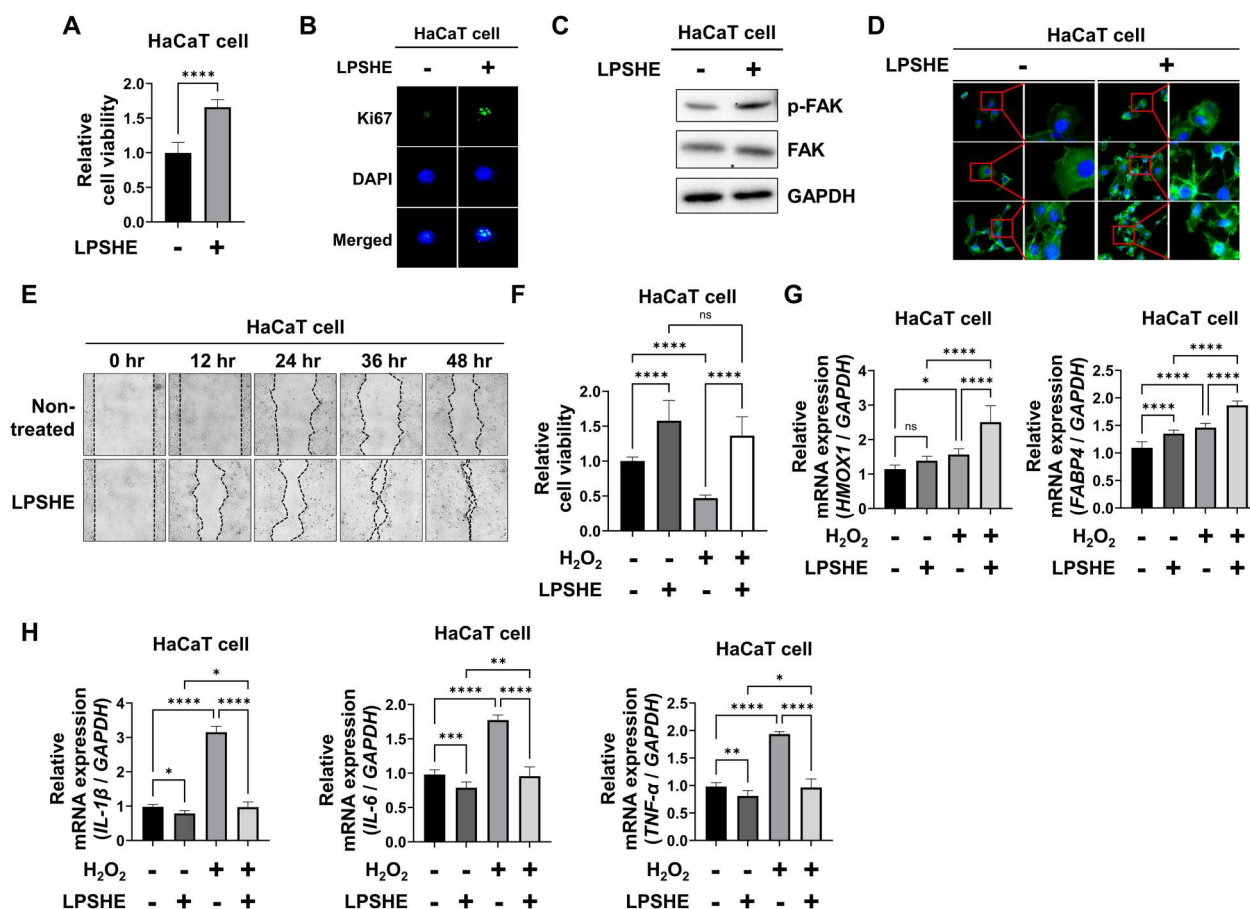


Figure 4. LPSHE enhances wound-healing ability in keratinocytes: (A) Alteration of cell viability treated with LPSHE (50 µg/mL, 24 h) in HaCaT cells. (B) Alteration of cell proliferation assessed by Ki-67 staining with LPSHE treatment (50 µg/mL, 24 h) in HaCaT cells. (C) Protein expression of FAK activation assessed by western blot analysis. (D) Distribution of filamentous actin with LPSHE treatment (50 µg/mL, 24 h) in HaCaT cells assessed by phalloidin staining (green: F-actin, blue: cell nuclei). (E) Motility and migration effects of LPSHE (50 µg/mL, 24 h) in HaCaT cells were analyzed using wound-healing scratch assays. Photomicrographs were taken at 100× magnification. (F) Alteration of antioxidation effect by LPSHE treatment (50 µg/mL, 24 h) in HaCaT cells. H₂O₂ was treated with 200 µg/mL, 24 h. (G) mRNA expression of HMOX1 and FABP4 with LPSHE treatment (50 µg/mL, 24 h) in HaCaT cells assessed by real-time qRT-PCR. H₂O₂ was treated with 200 µg/mL, 24 h. (H) mRNA expression of IL-1β, IL-6, and TNF-α with LPSHE treatment (50 µg/mL, 24 h) in HaCaT cells assessed by real-time qRT-PCR. H₂O₂ was treated with 200 µg/mL, 24 h. Statistical analysis was performed with one-way ANOVA plus a Dunnett's multiple comparisons test. ns; non-significant, *****p* < 0.0001.

results suggested that the LPSHE alleviates burn injury-induced hyperinflammation phenotypes.

LPSHE improves wound-healing capacity in human keratinocytes

To further verify the wound-healing capacity of the LPSHE-mediated wound-healing process in mouse models, we conducted *in vitro* experiments using human keratinocyte HaCaT cells. The LPSHE treatment increased the viability and proliferation of HaCaT cells (Figure 4(A and B)). The phosphorylation of FAK (Y397), which was involved in F-actin-mediated cytoskeletal remodeling, was increased by the LPSHE treatment (Figure 4(C)). We also observed that the filopodia formation contributed to cell migration (Figure 4(D)).

Through this LPSHE-induced wound-healing capacity, the LPSHE treatment accelerated the recovery of the wound area compared with the non-treated group, as assessed by the *in vitro* wound-healing scratch assay (Figure 4(E)). LPSHE also effectively reduced H₂O₂-induced cellular ROS toxicity (Figure 4(F)). Similar to the *in vivo* mouse model, the LPSHE enhanced HMOX1 and FABP4 expression levels (Figure 4(G)). Pro-inflammatory cytokines (IL-1β, IL-6, TNF-α) expression also decreased by the LPSHE treatment (Figure 4(H)). These results demonstrated that the LPSHE not only effectively regulated pro-inflammatory cytokines (first phase) but also increased the proliferative (second phase) and remodeling (third phase) phases through activation of the FAK signaling pathway to enhance the wound-healing capacity.

Discussion

The development of effective burn ointments is imperative for global healthcare. This study proposes new ingredients for burn ointments through the validation of the burn-healing efficacy of natural products extracted from *S. horneri*. Analysis of the wounded skin sections in a burn mouse model revealed that LPSHE restored the epidermis as well as the dermis (Figure 2 (C)). This result indicates that LPSHE could significantly heal third-degree burn wounds. In addition, this research demonstrated that LPSHE had an antioxidant effect on burn-injured skin or keratinocytes (Figure 2(F, G) and Figure 4(E)). Burn ointments with a ROS-regulatory effect can be used as a more effective treatment. Additionally, utilizing its ROS-regulatory effect, LPSHE could be also used as a possible therapeutic strategy for ROS-induced skin diseases, including photoaging (Petruk et al. 2018).

Previous studies have suggested the advantages of cryogrinding in natural product extraction (Nandasiri et al. 2019; Prasedya et al. 2021). In traditional Chinese herbal medicine, cryogrinding preserves the natural compounds with the highest purity (Singh and Goswami 2000; Munier et al. 2015; Saxena et al. 2018; Saluri et al. 2019). However, the amount of energy and cost of cryogrinding remains an unsuitable process for industrial-scale adjustment. To address the issue, we utilized LNG-based low-temperature pulverization, which was previously described in our study (Lee et al. 2021). Our LNG-powered system harnesses latent cold-state energy that requires heating before utilization. By utilizing our LNG-powered low-temperature pulverizing system, we investigated the novel *S. horneri* extract and demonstrated biological effects. From these results, we suggest that our LNG-powered low-temperature pulverizing system can increase the possibility of discovering novel bioactive compounds.

Upcycling is the transformation of waste into high-value products. Current upcycling technologies utilize chemical or engineering approaches to process plastic waste or polymers into high-value products (Choi et al. 2022; Jehanno et al. 2022; Lee et al. 2023). Harmful marine organisms have hazardous effects on the economy, aquaculture, and marine environment. *S. horneri* is also classified as a harmful marine organism. Over 10,000 tons of drifting *S. horneri* biomass, inflow from the Chinese coast to the Korean peninsula causes economic and environmental problems (Figure S2(A and B)) (Sanjeeva et al. 2019; Nagahawatta et al. 2021). Therefore, investigation of LPSHE biological effects could be a biological upcycling. From these results, we suggest that biological upcycling of harmful

marine organisms has the potential to discover novel bioactive compounds.

The results of the present study including LPSHE-induced inflammation attenuation and enhanced wound healing after burn injury suggested the role in burn wound repair and the molecular mechanism. In addition, we provided new insights that LPSHE can be utilized during burn treatment. We also suggested the importance of low-temperature pulverization systems in investigating novel bioactive compounds from marine organisms.

Material and methods

S. horneri low-temperature pulverization and characterization

The *S. horneri* was collected from Haenam county of Korea in June 2023 and stored at -60°C to prevent decay. Low-temperature pulverization machine is fabricated with stainless 304 steel and LNG injection with a relay controller. To control grinding temperature with the relay controller, a T-type thermocouple is attached in the upper part of the grinding chamber. The grinding blade type has two flat blades crossing each other. And grinding speed is 24,000 rpm. The cryogrinding process proceeds in the order of precooling to a target temperature of -60°C with liquefied natural gas (LNG) and operating the grinding motor after reaching the target temperature. During low-temperature pulverization, frictional heat raises the global temperature of the cryogrinding chamber, so the relay controller regulates liquid nitrogen flow to control temperature with a T-type thermocouple. HPLC analysis was performed by the Exion LC system and the PREF-LC system. All compounds are >95% pure by HPLC analysis. To characterize structural and molecular information based on LPSHE identification, Q-TOF LC/MS was performed by the SCIEX X500B Q-TOF system. In addition, proton nuclear magnetic resonance spectroscopy (NMR) was performed by Avance III 700.

Animal care protocol and establishment of a burn mouse model

Six-week-old male BALB/c nude mice (Orient Bio, Republic of Korea) were used for the *in vivo* experiments. The animal experiment protocols were approved by the Institutional Animal Care and Use Committee of Pusan National University (Approval Number PNU-2022-0060). *In vivo* experiments were performed under the guidelines of the National Institutes of Health's Guide for the Care and Use of Laboratory Animals. The mice were

kept at the animal care facilities placed on temperature-maintained room ($23 \pm 1^\circ\text{C}$) under a 12 h light/dark cycle and were fed commercial mouse chow and water. For burn injury, mice ($n=5$) were anesthetized and the dorsal hairs were clipped. The full-thickness burn wound was generated by 10 sec of contact with a 10-mm-diameter brass rod heated to 95°C . Mice were then administrated intraperitoneally with 1 mL of 37°C pre-warmed sterile isotonic saline to prevent shock symptom. After 1 day of burn wound generation, 500 mg of LPSHE and Commercial ointment was daily treated on mice burn-wounded area until the burn wound was fully recovered.

Treatment of LPSHE and commercial ointment

Purified LPSHE was prepared as a laboratory-grade ointment. 100 mg of LPSHE, glycerin, ethanol, and water per 1 g of ointment was appropriately mixed at room temperature. Burn-commercial ointment currently on the market, Madecassol Care Commercial ointment, was used as a positive control. Madecassol Care Commercial ointment mainly contains titrated extraction of *Centella Asiatica* 10 mg/g, neomycin sulfate 3.5 mg/g. And 500 mg of LPSHE and Commercial ointment was treated on mice burn-wounded area. Burn mouse group was treated with laboratory-grade ointment, which was excepted LPSHE as negative control.

Histological analysis

The tissue preparation protocol was validated as previously described (Son et al. 2019; Kim et al. 2023). At the end of the treatment period, animals were euthanized, and liver, lung, spleen, kidney, or skin samples were harvested. The samples were then fixed with formalin, dehydrated, and embedded in paraffin. Next, sections were cut into 4 mm and utilized for H&E, Masson's trichrome staining, or immunohistochemistry (IHC) following standard procedures. Stained sections were observed under an Olympus IX71 microscope (Olympus Optical, Japan). Inflammation scores were obtained as previously described (Seno et al. 2015). The inflammation conditions were evaluated using at least three H&E stained tissue sections, and IHC sections of the liver, lung, spleen, and kidney per mouse followed by the instructions described below. Inflammation scores were determined as follows: 0, no inflammation; 1, cellular infiltration only in the perivascular areas; 2, mild cellular infiltration (less than one-third part of the sections is infiltrated with inflammatory cells); 3, moderate cellular infiltration (more than one-third part of the sections is infiltrated with inflammatory cells); and 4,

infiltration of inflammatory cells is observed in the whole part of the sections.

Immunofluorescence and phalloidin staining

For HaCaT keratinocytes, the cells were fixed and permeabilized in cold acetone and then washed with cold PBS. For paraffinized tissue samples, deparaffinization was performed. After blocking with 1% BSA in PBS, the cells were incubated overnight with primary antibody at 4°C . Next, the cells were washed three times with cold PBS and incubated with DyLight 488-conjugated secondary antibodies (Thermo Fisher Scientific). After washing and counterstaining with DAPI (Sigma Aldrich), the glass slides were mounted with VECTA-SHIELD Hard-Set Mounting Medium (Vector Laboratories, Burlingame, CA) and visualized with an Olympus IX71 fluorescence microscope (Olympus Optical Co. Ltd., Tokyo, Japan). Phalloidin (Sigma Aldrich) staining was assessed according to the manufacturer's protocol.

ROS quantification

The DCFDA Cellular ROS Assay Kit was used (#ab113851, abcam) for detecting ROS levels. Around 100 μl of mouse blood sample or 1×10^4 of HaCaT cells were placed per well in 96-well plates. After appropriate treatments, incubated with the diluted DCFDA solution and Hoechst 33342 (#H3570, Invitrogen) for 1 h at 37°C protected from light. After incubation, the solutions were removed and 100 μl of buffer was added. Fluorescence was measured using a GloMax[®] Discover Microplate Reader at Ex/Em of 485/535 nm.

Cell culture

The culture methods of HaCaT cells were described in a previous study (Son et al. 2019). In detail, HaCaT cells were purchased from Korean Cell Line Bank (Seoul, Republic of Korea) and cultured in DMEM media consisting of 10% FBS and 1% penicillin (10,000 U/mL) – streptomycin (10,000 $\mu\text{g}/\text{mL}$) in a CO_2 incubator (37°C , 5% CO_2). Cells were free of mycoplasma contamination and were authenticated by short tandem repeat profiling within the past 12 months.

Wound-healing assay

Wound-healing assays were performed to measure changes in cell motility as previously described (Kim et al. 2016). In brief, HaCaT cells were cultured to 70% confluence and treated with LPSHE. The cell monolayers were then scratched with 200 μL pipette tips. Cells were

then further incubated for 24 or 48 h. Photomicrographs were then taken at 100× magnification using the Olympus IX71 fluorescence microscope (Olympus Optical Co. Ltd., Tokyo, Japan).

Total RNA isolation and qRT-PCR

Total RNA was extracted from HaCaT cells or mouse tissue with AccuPrep® Universal RNA Extraction Kit (#K-3140, bioneer, Korea). Synthesize cDNA was analyzed by Real-time qRT-PCR using an Applied Biosystems StepOne Real-Time PCR System (Applied Biosystems, USA). The qPCR primers sequences of the primers used are Mouse *Il1β* F: 5'-GCA ACT GTT CCT GAA CTC AAC T-3', R: 5'-ATC TTT TGG GGT CCG TCA ACT-3'. Mouse *Il6* F: 5'-GCT TAA TTA CAC ATG TTC TCT GGG AAA-3', R: 5'-CAA GTG CAT CAT CGT TGT TCA TAC-3'. Mouse *Tnf* F: 5'-TCG TAG CAA ACC ACC AAG TG-3', R: 5'-AGA TAG CAA ATC GGC TGA CG-3'. Mouse *Hmox1* F: 5'-AGG AGC TGC ACC GAA GGG CTG-3', R: 5'-CGT GGA GAC GCT TTA CAT AG-3'. Mouse *Fabp4* F: 5'-TCA CCA TCC GGT CAG AGA GTA-3', R: 5'-GCC ATC TAG GGT TAT GAT GCT C-3'. Mouse *Gapdh* F: 5'-CGA CTT CAA CAG CAA CTC CCA CTC TTC C-3', R: 5'-TGG GTG GTC CAG GGT TTC TTA CTC CTT-3'. Human *IL1β* F: 5'-TTC TTC GAC ACA TGG GAT AAC G-3', R: 5'-TCC CGG AGC GTG CAG TTC A-3'. Human *IL6* F: 5'-TGA ACT CCT TCT CCA CAA GCG-3', R: 5'-TCT TGG AGC TTA TTA AAG GCA TTC-3'. Human *TNF* F: 5'-CCG AGT GAC AAG CCT GTA GCC-3', R: 5'-CCT TGA AGA GGA CCT GGG AGT AG-3'. Human *HMOX1* F: 5'-CCA GGC AGA GAA TGC TGA GTT C-3', R: 5'-AAG ACT GGG CTC TCC TTG TTG C-3'. Human *FABP4* F: 5'-TTG ACG AAG TCA CTG CAG ATG A-3', R: 5'-CAG GAC ACC CCC ATC TAA. Human *GAPDH* F: 5'-ATG ACA TCA AGA AGG TGG TG-3', R: 5'-CAT ACC AGG AAA TGA GCT TG-3'. Each sample was assessed by triplication.

Western blot analysis

For acquiring the whole cell lysates, CETi Lysis Buffer with Inhibitors (TransLab, Korea) was used. The protein concentrations were determined by using a BioRad protein assay kit (BioRad Laboratories, USA). The protein samples were performed with SDS-PAGE, transferred to the NC (nitrocellulose) membrane, and blocked with 5% BSA in TBST for 2 h at room temperature. After incubation, membranes were treated with specific primary antibodies for overnight at 4°C. Washed with TBST and treated with peroxidase-conjugated secondary antibody (Thermo Fisher Scientific, USA). The membranes were visualized using an ECL detection system (Roche Applied Science, USA) with

iBright chemi-doc f1000 (Thermo Fisher Scientific, USA). Each analysis was assessed by triplication.

Cell viability assay

For cell viability assay, HaCaT cells were seeded at 10,000 cells per well in 96-well plates 1 d before treatment of LPSHE for 24 h. Cell viability was determined using Cell-Titer-Glo® Luminescent Viability Assay kit (#G7570, Promega).

Quantification and statistical analysis

All numerical data are presented as the means ± standard error of the mean from at least three independent experiments. For quantifications, a two-tail unpaired Student's *t*-test was used for comparing two experimental groups, and one-way ANOVA was applied when needed to compare three or more experimental groups. The log rank (Mantel–Cox) test was used for statistical analysis of survival. The Prism 9 software (GraphPad Software, San Diego, CA, USA) was used for all statistical analyses. A *p*-value <0.05 was considered to be statistically significant.

Acknowledgements

We thank WoojungBio Analysis Center (Seoul, Republic of Korea) for analyzing LC/MS–MS and NMR data. We also thank Editage for English language editing.

Ethic approval

The animal experiment protocols were approved by the Institutional Animal Care and Use Committee of Pusan National University (Approval Number PNU-2022-0060).

Disclosure statement

No potential conflict of interest was reported by the author(s).

Funding

This research was supported by Development and demonstration of on-board marine debris disposal modules program of Korea institute of Marine Science & Technology Promotion (KIMST), funded by the Ministry of Oceans and Fisheries (KIMST-20220494, J.-M.L. and B.Y.) and the '2024 Post-Doc. Development Program' of Pusan National University (E.S.).

Data availability statement

Data available on request from the authors.

References

- Balasubramanian S, Roselin P, Singh KK, Zachariah J, Saxena SN. 2016. Postharvest processing and benefits of black pepper, coriander, cinnamon, fenugreek, and turmeric spices. *Crit Rev Food Sci Nutr.* 56(10):1585–1607. Epub 2015/03/10. doi:10.1080/10408398.2012.759901.
- Burgess M, Valdera F, Varon D, Kankuri E, Nuutila K. 2022. The immune and regenerative response to burn injury. *Cells.* 11(19):3073. Epub 2022/10/15.
- Choi J, Yang I, Kim SS, Cho SY, Lee S. 2022. Upcycling plastic waste into high value-added carbonaceous materials. *Macromol Rapid Commun.* 43:e2100467. Epub 2021/10/14.
- Cragg GM. 1998. Paclitaxel (taxol): a success story with valuable lessons for natural product drug discovery and development. *Med Res Rev.* 18(5):315–331. Epub 1998/09/15. doi:10.1002/(SICI)1098-1128(199809)18:5<315::AID-MED3>3.0.CO;2-W.
- Engelhardt E, Toksoy A, Goebeler M, Debus S, Bröcker EB, Gillitzer R. 1998. Chemokines IL-8, GROalpha, MCP-1, IP-10, and mig are sequentially and differentially expressed during phase-specific infiltration of leukocyte subsets in human wound healing. *Am J Pathol.* 153(6):1849–1860. Epub 1998/12/10. doi:10.1016/S0002-9440(10)65699-4.
- Evers LH, Bhavsar D, Mailänder P. 2010. The biology of burn injury. *Exp Dermatol.* 19(9):777–783. Epub 2010/07/16. doi:10.1111/j.1600-0625.2010.01105.x.
- Freitas MV, Pacheco D, Cotas J, Mouga T, Afonso C, Pereira L. 2022. Red seaweed pigments from a biotechnological perspective. *Phycology.* 2(1):1–29.
- Furuhashi M, Saitoh S, Shimamoto K, Miura T. 2014. Fatty acid-binding protein 4 (FABP4): pathophysiological insights and potent clinical biomarker of metabolic and cardiovascular diseases. *Clin Med Insights Cardiol.* 8:23–33. Epub 2015/02/13.
- Gurtner GC, Werner S, Barrandon Y, Longaker MT. 2008. Wound repair and regeneration. *Nature.* 453(7193):314–321. Epub 2008/05/16. doi:10.1038/nature07039.
- Haase I, Evans R, Pofahl R, Watt FM. 2003. Regulation of keratinocyte shape, migration and wound epithelialization by IGF-1- and EGF-dependent signalling pathways. *J Cell Sci.* 116(15):3227–3238. Epub 2003/06/28. doi:10.1242/jcs.00610.
- Han EJ, Kim SY, Han HJ, Kim HS, Kim KN, Fernando IPS, Madusanka DMD, Dias M, Cheong SH, Park SR, et al. 2021. UVB protective effects of *Sargassum horneri* through the regulation of Nrf2 mediated antioxidant mechanism. *Sci Rep.* 11(1):9963. Epub 2021/05/13. doi:10.1038/s41598-021-88949-3.
- Herath K, Kim HJ, Lee JH, Je JG, Yu HS, Jeon YJ, Kim HJ, Jee Y. 2021. *Sargassum horneri* (turner) C. Agardh containing polyphenols attenuates particulate matter-induced inflammatory response by blocking TLR-mediated MYD88-dependent MAPK signaling pathway in MLE-12 cells. *J Ethnopharmacol.* 265:113340. Epub 2020/09/07. doi:10.1016/j.jep.2020.113340.
- James SL, Lucchesi LR, Bisignano C, Castle CD, Dingels ZV, Fox JT, Hamilton EB, Henry NJ, McCracken D, Roberts NLS, et al. 2020. Epidemiology of injuries from fire, heat and hot substances: global, regional and national morbidity and mortality estimates from the global burden of disease 2017 study. *Inj Prev.* 26(Suppl2):i36–i45. Epub 2019/12/21. doi:10.1136/injuryprev-2019-043299.
- Jehanno C, Alty JW, Roosen M, De Meester S, Dove AP, Chen EY, Leibfarth FA, Sardon H. 2022. Critical advances and future opportunities in upcycling commodity polymers. *Nature.* 603(7903):803–814. Epub 2022/04/01. doi:10.1038/s41586-021-04350-0.
- Jeschke MG, van Baar ME, Choudhry MA, Chung KK, Gibran NS, Logsetty S. 2020. Burn injury. *Nat Rev Dis Primers.* 6(1):11. Epub 2020/02/15. doi:10.1038/s41572-020-0145-5.
- Jung H, Jung DM, Lee SS, Kim EM, Yoon K, Kim KK. 2022. *Mangifera Indica* leaf extracts promote hair growth via activation of Wnt signaling pathway in human dermal papilla cells. *Animal Cells Syst (Seoul).* 26(3):129–136. Epub 2022/07/06. doi:10.1080/19768354.2022.2085790.
- Jung JY, Rhee JK. 2020. Roasting and cryogenic grinding enhance the antioxidant property of sword beans (*Canavalia gladiata*). *J Microbiol Biotechnol.* 30(11):1706–1719. Epub 2020/08/25. doi:10.4014/jmb.2003.03069.
- Kim B, Kim JS, Youn B, Moon C. 2023. Dopamine depletion alters neuroplasticity-related signaling in the rat hippocampus. *Animal Cells Syst (Seoul).* 27(1):436–446. Epub 2023/12/21. doi:10.1080/19768354.2023.2294308.
- Kim JY, Jang S, Song HJ, Lee S, Cheon S, Seo EJ, Choi YH, Kim SH. 2024. *Sargassum horneri* extract fermented by *Lactiplantibacillus pentosus* SH803 mediates adipocyte metabolism in 3T3-L1 preadipocytes by regulating oxidative damage and inflammation. *Sci Rep.* 14(1):15064. Epub 2024/07/03. doi:10.1038/s41598-024-65956-8.
- Kim W, Kim E, Lee S, Kim D, Chun J, Park KH, Youn H, Youn B. 2016. TFAP2C-mediated upregulation of TGFBR1 promotes lung tumorigenesis and epithelial-mesenchymal transition. *Exp Mol Med.* 48:e273. Epub 2016/11/26.
- Krishnaswamy VR, Korrapati PS. 2014. Role of dermatopontin in re-epithelialization: implications on keratinocyte migration and proliferation. *Sci Rep.* 4(1):7385. Epub 2014/12/10. doi:10.1038/srep07385.
- Lee DH, Park S, Kim HT, Kim JD, Kim JH, Kim SK, Seo JK, Song PK, Oh JE, Youn B, et al. 2021. Proposing a new solution for marine debris by utilizing on-board low-temperature eco-friendly pulverization system. *Sci Rep.* 11(1):24364. Epub 2021/12/23. doi:10.1038/s41598-021-03757-z.
- Lee HS, Jung S, Lin KA, Kwon EE, Lee J. 2023. Upcycling textile waste using pyrolysis process. *Sci Total Environ.* 859:160393. Epub 2022/11/25. doi:10.1016/j.scitotenv.2022.160393.
- Lee JH, Kim HJ, Jee Y, Jeon YJ, Kim HJ. 2020. Antioxidant potential of *Sargassum horneri* extract against urban particulate matter-induced oxidation. *Food Sci Biotechnol.* 29(6):855–865. Epub 2020/06/12. doi:10.1007/s10068-019-00729-y.
- Lim C, Lim J, Choi S. 2023. Wound-induced hair follicle neogenesis as a promising approach for hair regeneration. *Mol Cells.* 46(10):573–578. Epub 2023/08/31. doi:10.14348/molcells.2023.0071.
- Lima CF, Pereira-Wilson C, Rattan SI. 2011. Curcumin induces heme oxygenase-1 in normal human skin fibroblasts through redox signaling: relevance for anti-aging intervention. *Mol Nutr Food Res.* 55(3):430–442. Epub 2010/10/13. doi:10.1002/mnfr.201000221.
- Liu H, Zheng J, Liu P, Zeng F. 2018. Pulverizing processes affect the chemical quality and thermal property of black, white, and green pepper (*piper nigrum* L.). *J Food Sci Technol.* 55(6):2130–2142. Epub 2018/06/13. doi:10.1007/s13197-018-3128-8.

- Lomartire S, Gonçalves AMM. 2023. Marine macroalgae polyphenols as potential neuroprotective antioxidants in neurodegenerative diseases. *Mar Drugs*. 21(5):261. Epub 2023/05/26.
- Matulja D, Wittine K, Malatesti N, Laclef S, Turks M, Markovic MK, Ambrožić G, Marković D. 2020. Marine natural products with high anticancer activities. *Curr Med Chem*. 27:1243–1307. Epub 2020/01/15.
- Mittal M, Siddiqui MR, Tran K, Reddy SP, Malik AB. 2014. Reactive oxygen species in inflammation and tissue injury. *Antioxid Redox Signal*. 20(7):1126–1167. Epub 2013/09/03. doi:10.1089/ars.2012.5149.
- Munier M, Moranças M, Dumay J, Jaouen P, Fleurence J. 2015. One-step purification of R-phycoerythrin from the red edible seaweed *Grateloupia turuturu*. *J Chromatogr B*. 992:23–29. doi:10.1016/j.jchromb.2015.04.012.
- Nagahawatta DP, Kim HS, Jee YH, Jayawardena TU, Ahn G, Namgung J, Yeo IK, Sanjeeva KKA, Jeon YJ. 2021. Sargachromenol isolated from *Sargassum horneri* inhibits particulate matter-induced inflammation in macrophages through toll-like receptor-mediated cell signaling pathways. *Mar Drugs*. 20(1):28. Epub 2022/01/21. doi:10.3390/md20010028.
- Nandasiri R, Eskin NAM, Thiyam-Höllander U. 2019. Antioxidative polyphenols of canola meal extracted by high pressure: impact of temperature and solvents. *J Food Sci*. 84(11):3117–3128. Epub 2019/10/31. doi:10.1111/1750-3841.14799.
- Parihar A, Parihar MS, Milner S, Bhat S. 2008. Oxidative stress and anti-oxidative mobilization in burn injury. *Burns*. 34(1):6–17. Epub 2007/10/02. doi:10.1016/j.burns.2007.04.009.
- Peña OA, Martin P. 2024. Cellular and molecular mechanisms of skin wound healing. *Nat Rev Mol Cell Biol*. 25(8):599–616. Epub 2024/03/26.
- Peñalver R, Lorenzo JM, Ros G, Amarowicz R, Pateiro M, Nieto G. 2020. Seaweeds as a functional ingredient for a healthy diet. *Mar Drugs*. 18(6):301. Epub 2020/06/11.
- Petruk G, Del Giudice R, Rigano MM, Monti DM. 2018. Antioxidants from plants protect against skin photoaging. *Oxid Med Cell Longev*. 2018(1):1454936. Epub 2018/09/04.
- Prasedya ES, Frediansyah A, Martyasari NWR, Ilhami BK, Abidin AS, Padmi H, Fahrurrozi, Juansilfero AB, Widyastuti S, Sunarwidhi AL. 2021. Effect of particle size on phytochemical composition and antioxidant properties of *Sargassum cristaefolium* ethanol extract. *Sci Rep* 11(1):17876. Epub 2021/09/11. doi:10.1038/s41598-021-95769-y.
- Rivera-Gonzalez G, Shook B, Horsley V. 2014. Adipocytes in skin health and disease. *Cold Spring Harb Perspect Med*. 4(3):a015271. Epub 2014/03/05.
- Rodrigues M, Kosaric N, Bonham CA, Gurtner GC. 2019. Wound healing: a cellular perspective. *Physiol Rev* 99(1):665–706. Epub 2018/11/27. doi:10.1152/physrev.00067.2017.
- Saluri M, Kaldmäe M, Tuvikene R. 2019. Extraction and quantification of phycobiliproteins from the red alga *Furcellaria lumbricalis*. *Algal Res* 37:115–123. doi:10.1016/j.algal.2018.11.013.
- Sanjeeva KKA, Jayawardena TU, Kim SY, Lee HG, Je JG, Jee Y, Jeon YJ. 2020. *Sargassum horneri* (Turner) inhibit urban particulate matter-induced inflammation in MH-S lung macrophages via blocking TLRs mediated NF-κB and MAPK activation. *J Ethnopharmacol*. 249:112363. Epub 2019/11/05. doi:10.1016/j.jep.2019.112363.
- Sanjeeva KKA, Jayawardena TU, Lee HG, Herath K, Jee Y, Jeon YJ. 2019. The protective effect of *Sargassum horneri* against particulate matter-induced inflammation in lung tissues of an in vivo mouse asthma model. *Food Funct*. 10(12):7995–8004. Epub 2019/12/04. doi:10.1039/C9FO02068C.
- Saxena SN, Barnwal P, Balasubramanian S, Yadav DN, Lal G, Singh KK. 2018. Cryogenic grinding for better aroma retention and improved quality of Indian spices and herbs: a review. *J Food Process Eng*. 41:e12826.
- Seno A, Maruhashi T, Kaifu T, Yabe R, Fujikado N, Ma G, Ikarashi T, Kakuta S, Iwakura Y. 2015. Exacerbation of experimental autoimmune encephalomyelitis in mice deficient for DCIR, an inhibitory C-type lectin receptor. *Exp Anim*. 64(2):109–119. Epub 2015/07/16.
- Sharma LK, Agarwal D, Rathore SS, Malhotra SK, Saxena SN. 2016. Effect of cryogenic grinding on volatile and fatty oil constituents of cumin (*Cuminum cyminum* L.) genotypes. *J Food Sci Technol*. 53(6):2827–2834. Epub 2016/08/02. doi:10.1007/s13197-016-2258-0.
- Singh KKK, Goswami TK. 2000. Cryogenic grinding of cloves. *J Food Process Eng*. 24:57–71.
- Son B, Lee S, Kim H, Kang H, Kim J, Youn H, Nam SY, Youn B. 2019. Low dose radiation attenuates inflammation and promotes wound healing in a mouse burn model. *J Dermatol Sci*. 96(2):81–89. Epub 2019/11/11. doi:10.1016/j.jdermsci.2019.10.004.
- Song KH, Jung SY, Kho SH, Hwang SG, Ha H, Nam SY, Song JY. 2017. Effects of low-dose irradiation on mice with *Escherichia coli*-induced sepsis. *Toxicol Appl Pharmacol*. 333:17–25. Epub 2017/08/19. doi:10.1016/j.taap.2017.08.008.
- Tiwari VK. 2012. Burn wound: how it differs from other wounds? *Indian J Plast Surg*. 45(2):364–373. Epub 2012/11/20. doi:10.4103/0970-0358.101319.
- Werner S, Krieg T, Smola H. 2007. Keratinocyte-fibroblast interactions in wound healing. *J Invest Dermatol*. 127(5):998–1008. Epub 2007/04/17. doi:10.1038/sj.jid.5700786.
- Yuan Y, Zhong S, Deng Z, Li G, Li H. 2023. Impact of particle size on the nutrition release and antioxidant activity of rape, buckwheat and rose bee pollens. *Food Funct*. 14(4):1897–1908. Epub 2023/02/02. doi:10.1039/D2FO03119A.
- Żwieręto W, Piorun K, Skórka-Majewicz M, Maruszewska A, Antoniewski J, Gutowska I. 2023. Burns: classification, pathophysiology, and treatment: a review. *Int J Mol Sci*. 24(4):3749. Epub 2023/02/26.